

Microstructural Evolution and Structure-Hardness Relationship in an Al-4wt.%Mg Alloy Processed by High-Pressure Torsion

Xiaohui Yang, Jianhong Yi, Song Ni, Yong Du, and Min Song

(Submitted January 5, 2016; in revised form March 11, 2016; published online April 11, 2016)

Coarse-grained Al-4wt.%Mg alloy with high stacking fault energy was deformed by high-pressure torsion (HPT) at room temperature. The HPT-induced grain refinement process of the alloy can be clarified as follows: (1) the randomly distributed dislocations firstly interact and rearrange to form dislocation cells; (2) with increasing the strain, these cell boundaries transform to small-angle grain boundaries that act as the dislocation sources, and therefore Shockley partial dislocations on the glide plane (111) can be easily emitted to accommodate plastic deformation; (3) along with the partial dislocations emission from low angle grain boundaries, the low angle grain boundaries gradually transform into the high angle grain boundaries. The relationship between the microstructural evolution and hardness was also investigated. It has been shown that the relationship between grain size and hardness deviates from the Hall-Petch linear relationship.

Keywords Al-Mg alloy, Hall-Petch relationship, high-pressure torsion, partial dislocation

1. Introduction

Ultrafine-grained (UFG) and nanocrystalline (NC) materials have attracted extensive attention due to their excellent mechanical properties (Ref 1). Severe plastic deformation (SPD) techniques, including equal channel angular pressing (ECAP) (Ref 2), high-pressure torsion (HPT) (Ref 3), multi-axial compression (MAC) (Ref 4), accumulative roll-bonding (ARB) (Ref 5), and twist extrusion (TE) (Ref 6, 7) have been widely used to fabricate bulk UFG and NC materials (Ref 8, 9). Among all these SPD techniques, HPT is very attractive because of its ability to achieve extremely high applied pressures and consequent production of exceptional grain refinement (Ref 3). To date, HPT has been used to process many different metallic materials and three models of hardness evolution have been concluded for the ultrafine-grained materials processed by HPT (Ref 10). It is noteworthy that the nanostructured Al alloys with excellent mechanical properties have been largely investigated by HPT in the last decade (Ref 11). In addition, the nanoscale structural elements (dislocation boundaries, stacking faults, and nanotwins) can be identified in the deformation process for UFG Al alloys induced by HPT. The nanoscale structural elements have a considerable effect on the mechanical behavior, and a better understanding of the evolution mechanisms of these nanoscale structural elements in Al alloys during HPT process can enable improvements of the

mechanical properties. Therefore, it is necessary to further investigate the microstructural evolution and strengthening mechanism of Al alloys processed by HPT.

It has been widely reported that for metals and alloys with medium stacking fault energy (SFE) (Ref 12, 13) or low SFE (Ref 14), deformation mechanism transforms from dislocation slip to twinning when the grain was refined from micron size to ultrafine or nanometer size. For pure Al or Al alloys with high SFE, Chen et al. (Ref 15) and Liao et al. (Ref 16) indicated the occurrence of twinning in NC Al alloy subjected to large plastic strain. In addition, Liu et al. (Ref 17) observed nanotwins and stacking faults in Al-Mg alloys processed by HPT, and Li et al. (Ref 18) verified that nanotwins can form in coarse-grained Al alloy at ambient temperature and low strain rate due to the high local stress. Recently, Cao et al. (Ref 19) confirmed that applied stress rather than grain size controls the production of nanotwins during HPT processing coarse-grained duplex steel with low SFE. In addition, although the addition of Mg to Al decreases the SFE, 4wt.%Mg addition to Al only reduces the SFE from ~ 166 mJ/m² (Ref 6) to ~ 120 mJ/m² (Ref 7). Therefore, a question is raised: how does the applied stress affect the microstructural evolution of Al-4wt.%Mg alloy with high SFE? In this paper, an Al-4wt.%Mg alloy was subjected to HPT at room temperature. The objectives of this work are to understand: (1) how the original coarse grains are refined into much smaller structural elements at low strain; (2) how the high flow stress affects the microstructural evolutions at intermediate and large plastic strains, and (3) how the structural evolution affects the hardness? The answers to these questions provide a basis for understanding the grain refinement process of Al-4wt.% Mg alloy with high SFE.

2. Experimental

The material used in present work is an Al-4wt.%Mg alloy fabricated by ingot metallurgy, in which commercially pure Al and Mg (both are 99.9 wt.% in purity) were used as the raw

Xiaohui Yang, Song Ni, Yong Du, and Min Song, State Key Laboratory of Powder Metallurgy, Central South University, Changsha 410083, China; and Jianhong Yi, School of Materials Science and Engineering, Kunming University of Science and Technology, Kunming 650093, China. Contact e-mail: msong@csu.edu.cn.

materials. The alloy was then homogenization annealed at 733 K for 10 h. The average grain size was $\sim 400 \mu\text{m}$ in the annealed alloy according to optical microscope observation. Specimens for HPT processing were sectioned into disks from the annealed alloy with a diameter of slightly less than 20 mm and a thickness of $\sim 2 \text{ mm}$. These disks were polished on both sides using sand papers (400-2000 grade) until their thickness reached $\sim 1.7 \text{ mm}$. Then, the HPT process was conducted using a quasi-constrained HPT facility (Ref 3). Disks were subjected to 1-, 3-, 5-, and 10-turns HPT under an applied pressure of 4 GPa and a rotation rate of 1 turn per minute, respectively.

After HPT processing, the disks were mechanically polished to produce a mirror-like surface using diamond lapping films for hardness testing. Hardness measurements were carried out by an FEI-VM50 PC Vickers hardness testing machine at room temperature using 50 g load and 15 s dwell time. The hardness was measured at points with radius values from 1 to 9.5 mm separated by 0.5 mm and the hardness value for each radius value was averaged from 8 datum points positioned by a rotational increment of 45° around the disk center. The hardness value at the disk center and at a radius value of 0.5 mm were averaged from 3 datum points by a rotational increment of 120° and from 4 datum points by a rotational increment of 90° around the disk center, respectively. The points in a disk where hardness was tested are shown schematically in Fig. 1(a). TEM samples were prepared by a twin-jet polishing technique in a mixture of 30% nitric acid and 70% carbinol at -30°C . The TEM investigations were carried out using a JEOL 2100F microscope operating at 200 kV. In order to facilitate discussion, the locations for TEM foil specimen preparation were named regions I, II, and III, as shown in Fig. 1(b).

3. Results

3.1 Hardness Evolution

Figure 2 shows the hardness evolution of the disks subjected to 1, 3, 5, and 10 turns as a function of the radius. The Vickers

hardness increases from 64 Hv in the as-annealed state to 87 Hv at the center of 1-turn HPT disk. In the early stage of HPT processing, the hardness distribution is characterized by low values in the central region and much higher values in regions close to the periphery of the disks. With increasing the turns introduced by further HPT processing, the hardness at the central region increases and the difference in the hardness between the central and the periphery regions becomes smaller. Meanwhile, the hardness in the region with a radius larger than 5 mm for 5- and 10-turns treated disks is reasonably uniform with some fluctuations between 200 and 220 Hv. Owing to strain non-uniformity inherent in HPT (Ref 3), strain gradients become a significant feature of the deformation process. Recently, the more and more uniform microstructure occurring in HPT samples with increasing torsional straining has been successfully modeled using strain gradient plasticity theory (Ref 20), which explains the decrease in the hardness difference between the center and the edge of the disks with increasing HPT turns.

3.2 Microstructural Evolution

3.2.1 Microstructural Evolution at Low Strain. Figure 3 shows a TEM micrograph of an initial grain with $1.2 \mu\text{m}$ in length and $0.7 \mu\text{m}$ in width at region I after 3-turns. Areas 1 and 2 are divided by a low-angle grain boundary marked by a pair of white arrows. The low-angle grain boundary was formed by the accumulation of a number of glide dislocations. Dislocation tangling is also observed in the interior of grains, as marked by a white circle in Fig. 3(a), which is usually named as dislocation tangle zone (DTZ) (Ref 21). A subgrain surrounded by a white box inside the large grain is usually called isolated subgrain and its main feature includes a very high density of dislocation stored inside the subgrain (Ref 21). Figure 3(b) is the high-resolution TEM (HRTEM) image of the region along $[110]$ direction marked by the red arrow. The inverse Fourier transformation image of Fig. 3(b) demonstrates that a lot of dislocations marked by black “T” on (111) plane are stored in the area, as shown in Fig. 3(c). The dislocation pile-up at the border arouses a small misorientation between area 2 and area 3. Figure 3(d) shows the HRTEM image of the area marked by

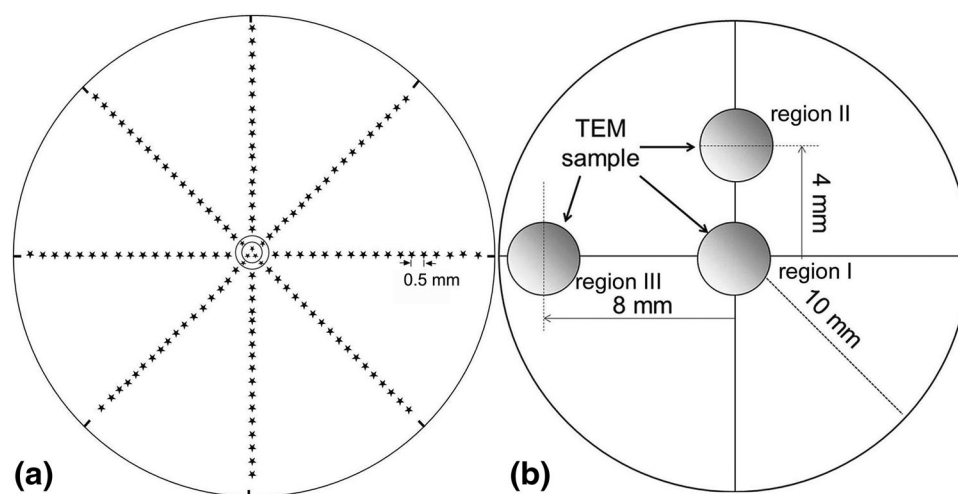


Fig. 1 (a) Schematic illustration of the procedure for hardness measurements across the diameters of disks after HPT and (b) the regions cut from the disks subjected to different HPT turns for TEM observations, i.e., the center region at $r = 0$ marked as I, and the regions at $r = 4 \text{ mm}$ and $r = 8 \text{ mm}$ marked as II and III, respectively

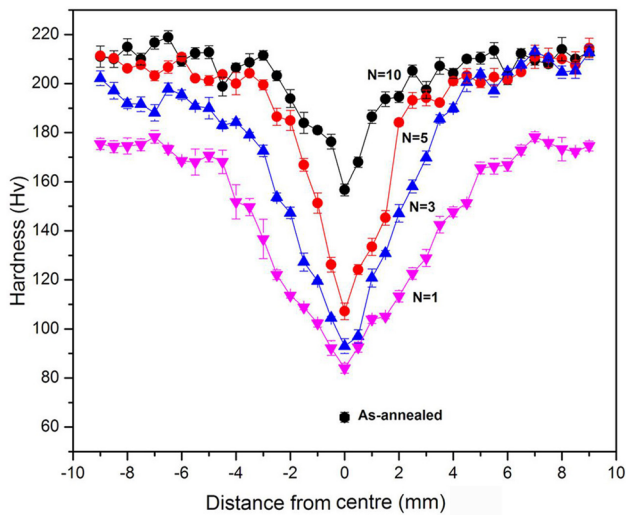


Fig. 2 (a) The average Vickers hardness as a function of the radius after HPT processing for 1, 3, 5, and 10 turns

a pair of white arrows. The fast Fourier transformation (FFT) pattern of the area as an inset in Fig. 3(d) shows two sets of diffraction spots and the misorientation between area 1 and area 2 is 8° . Figure 3(e) is the inverse Fourier transformation pattern of Fig. 3(d). An obvious feature is that dislocations in the (111) plane distribute more orderly compared to that in Fig. 3(c). Obviously, dislocation interaction and annihilation at the boundary changed the misorientation of adjacent regions and facilitated the coarse grain refinement.

3.2.2 Microstructural Evolution at Large Strain. With increasing the strain, the grains can be refined to ultrafine scale or nanometer scale. Figure 4 demonstrates a unique microstructure formed at region II after 3 turns. Figure 4(a) shows that a grain with the size of about 500 nm has been subdivided to several domains marked by white dashed lines. Figure 4(b) demonstrates a very high density of the stacking faults ($\sim 2.5 \times 10^{15} \text{ m}^{-2}$) in the grain, which is far more than that observed in the sample subjected to multi-axial compression (Ref 22). The higher density of stacking fault in this work compared to that of MAC processed sample may be caused by higher shear stress during HPT process. It is well known that dislocation multiplication from Frank-Read sources becomes difficult and the partial dislocation emission from the ultrafine grain boundary becomes the primary deformation mechanism when the grain size is refined to ultrafine or nanometer scale (Ref 23). Because of several hundred nanometers of the subgrain size in this study, the propensity for dislocation nucleation from Frank-Read sources decreases, while the propensity for partial dislocation emission from the boundary increases (Ref 24). Previous study showed that the resolved shear stress to move a full dislocation from a grain boundary into a grain is greater than the stress required to extend a partial dislocation into the same grain for f.c.c. metals with a small grain size (Ref 25). Moreover, the local stress is significantly different from the global shear stress due to the stress concentration by atomistic simulation (Ref 26). So, the increment in applied stress required to continue deformation in small volumes favors partial dislocation emission from local region in the boundary of the grain rather than full dislocation slip since the latter requires larger shear stress (Ref 24).

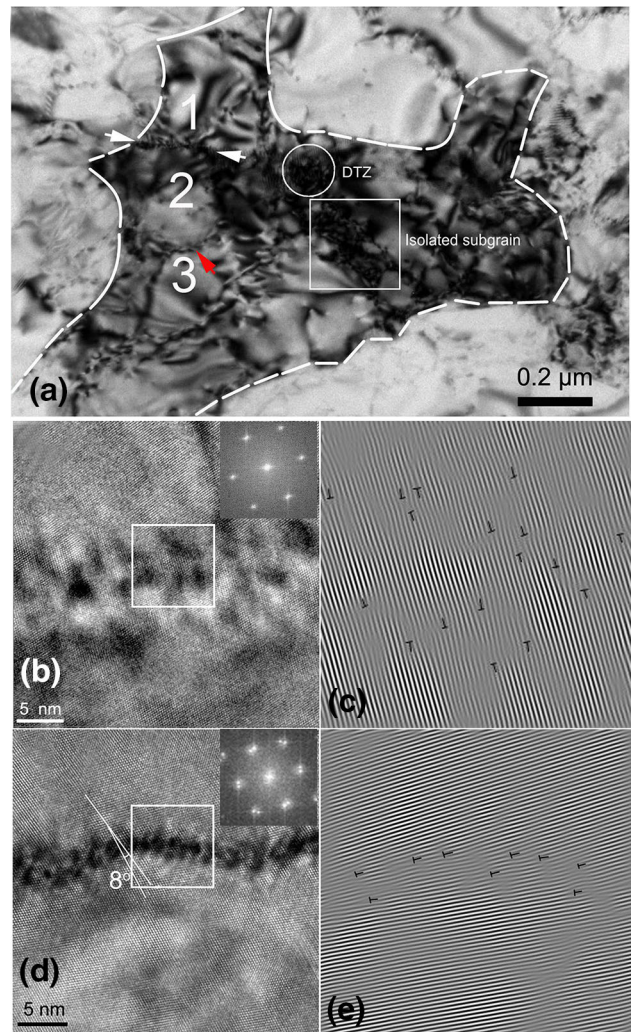


Fig. 3 (a) A TEM micrograph of a coarse-grain at region I after 3-turns, with the numbers 1-3 denoting three regions, (b) an HRTEM image of the piled-up dislocations in the boundary between two adjacent cell blocks (2 and 3), (c) a Fourier filtered image of the rectangular region in (b) with the dislocations being indicated by black “T,” (d) an HRTEM image of the low-angle grain boundary between regions 1 and 2 and (e) a Fourier filtered image of the rectangular region in (d) with the dislocations being indicated with black “T”

Figure 5 shows bright field TEM images and the distribution bar graphs of the grain size in region III of the disks after HPT for 1, 3, 5, 10 turns. Comparing the microstructure in Fig. 5(a, c, e and g), an obvious feature is that the grain boundaries become clearer and sharper. In order to carefully study the grain size evolution in region III after different turns, the distribution bar graphs of the grain size in region III after 1, 3, 5, and 10 HPT turns are shown in Fig. 5(b, d, f, and h). It can be seen that the grain size is mainly distributed in the range of 50-250 nm at region III after different HPT turns and the average values of grain size after 1, 3, 5, 10, turns are 145, 110, 100, and 90 nm. Comparing the grain size distribution of different turns, it is obvious that with increasing the HPT turns, the grain size distribution is more uniform. Similarly, the average values of grain size from regions I and II after different turns are counted

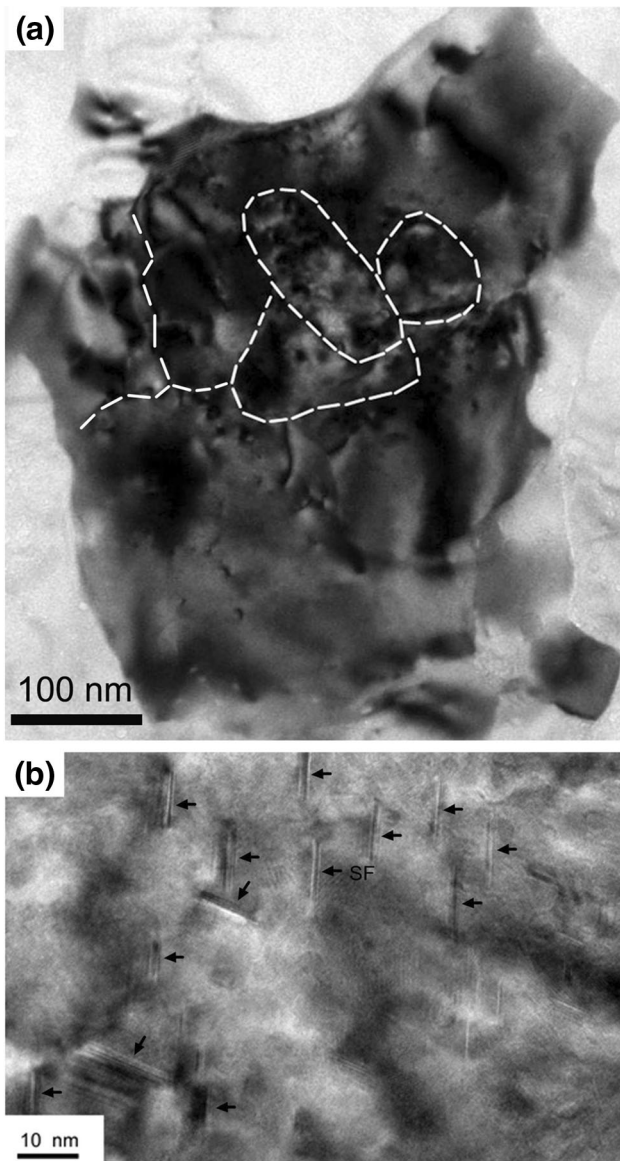


Fig. 4 (a) A TEM micrograph demonstrates that some nanodomains exist inside a several hundred nanometer grain and (b) a lot of partial dislocation bounding stacking faults was observed in the nanodomains

based on the microstructure observation by TEM and are summarized in Table 1.

4. Discussion

4.1 The Grain Refinement Process

In this work, dislocation tangles, nanotwins or stacking faults are observed during the grain refinement process of Al-4wt.%Mg alloy induced by HPT. At the initial stage of deformation, plastic deformation is dominated by dislocation accumulation, interaction, tangling and spatial rearrangement. As demonstrated in Fig. 3, coarse-grain refinement is dominated by the well-known dislocation subdivision mechanism (Ref 2). With further straining, nanodomains form inside the ultrafine grain, as shown in Fig. 4(a). When the stress surpasses

the critical stress for partial dislocation emission, the partial dislocations are emitted from the boundaries of the nanodomains and the nanodomains gradually transform into superfine or nanometer grains. In short, the refinement process can be summarized as follows: (1) the randomly distributed dislocations firstly interacted and rearranged to form dislocation cells; (2) with increasing the strain, these cell boundaries transformed to small-angle grain boundaries that act as the dislocation sources, and therefore, in these small-angle grain boundaries with large local shear stress, Shockley partial dislocations on the glide plane (111) of the ultrafine grain can be easily emitted in order to accommodate plastic deformation; (3) along with partial dislocations emission from grain boundary, the subgrains with low angle grain boundaries gradually transform into high angle grain boundaries.

4.2 The Influence of Structural Evolution on Hardness

The relationship between the hardness (H) of a completely recrystallized polycrystalline material and its average grain size (d) can be described by the Hall-Petch equation (Ref 27):

$$H = H_0 + K_H d^{-1/2},$$

where H_0 and K_H are the material constants. The average grain size is counted based on the high-angle grain boundaries. However, the microstructure of materials during plastic deformation often consists of various substructures, such as low-angle boundaries or dislocation walls/tangles. Therefore, investigating the influence of substructural evolution during SPD process on hardness have aroused a lot of interesting. For example, Hansen (Ref 28) proposed that for deformed metals, boundary strengthening is not a constant and the contribution for hardness from dislocation in the grain interior can be neglected in pure metals with medium or high stacking fault energy.

Figure 6 shows the hardness values of Al-4wt.%Mg alloy obtained at three regions of the disks after 1, 3, 5, and 10 turns as a function of $d^{-1/2}$ (the measurement of d including both the high angle grain boundaries and low angle grain boundaries), together with the initial coarse grain size and hardness obtained from the undeformed specimen. It can be seen that these hardness values corresponding to different grain sizes and substructures do not follow the Hall-Petch correlation very well. At low strain, the hardness values surpass the predicted values and at medium strain the hardness values are less than that predicted from the Hall-Petch equation. It is well known that hardening in metals and alloys induced through plastic deformation originates from grain size refinement and dislocation density increase. A lot of experiments have shown that dislocations can rapidly multiply in coarse grains but is difficultly stored in ultrafine grains or nanograins (Ref 8, 29). Therefore, the contribution from intragranular dislocations can be ignored when the grain size is refined to submicrometer level or less, and grain boundary structure plays a more important role on the hardness evolution (Ref 8). As shown in Fig. 6(a), a dark field image for the microstructure is characterized by a lot of dislocation lines stored inside the grain interior at low strain. With increasing the strain, intragranular dislocations decrease and a lot of grain boundaries are composed of dislocation boundaries, as shown in Fig. 6(b). The significance of grain boundary characteristics in tailoring the mechanical strength of metals was noted earlier for conventional coarse-grained materials, where it was shown that a higher fraction of special

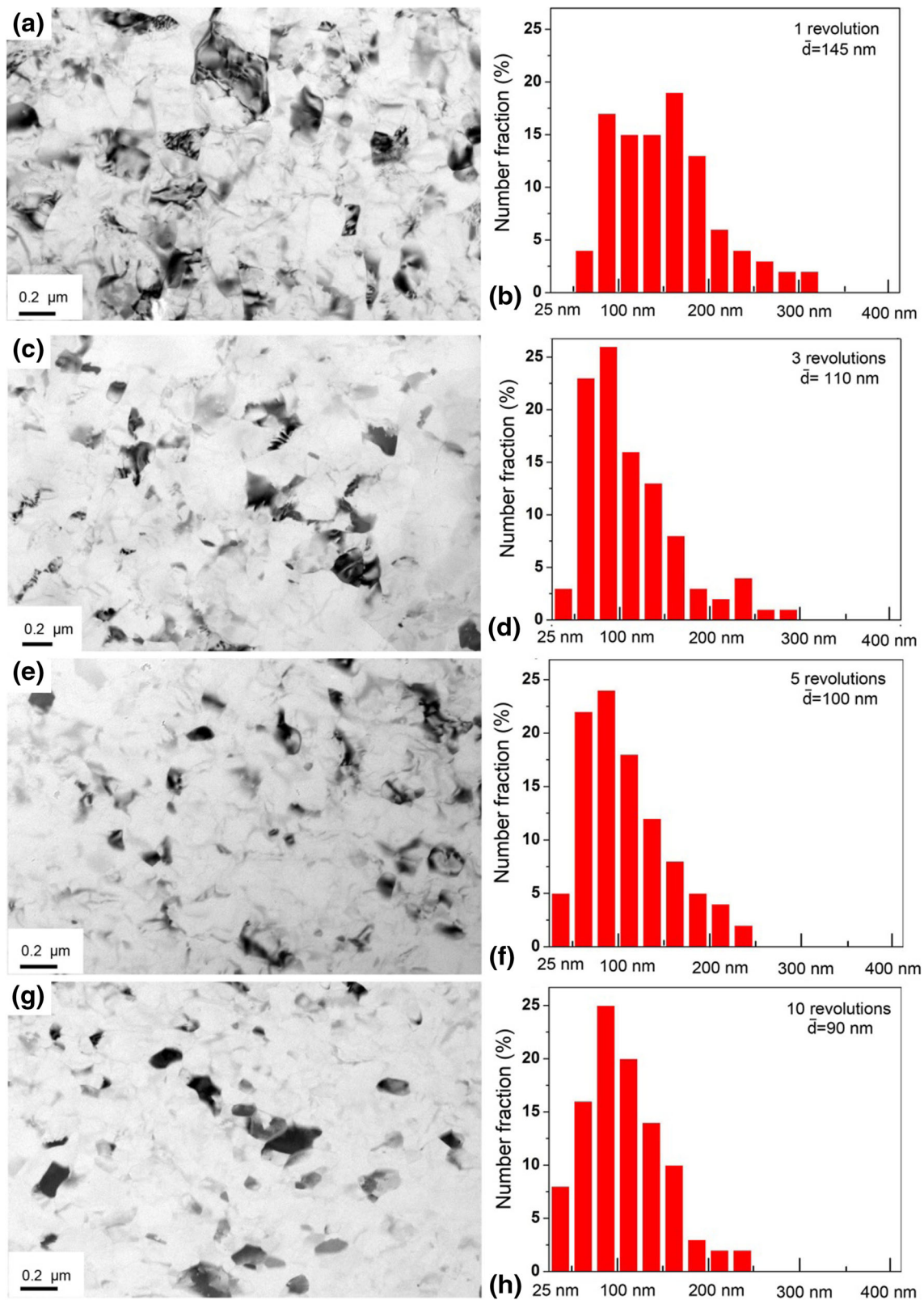


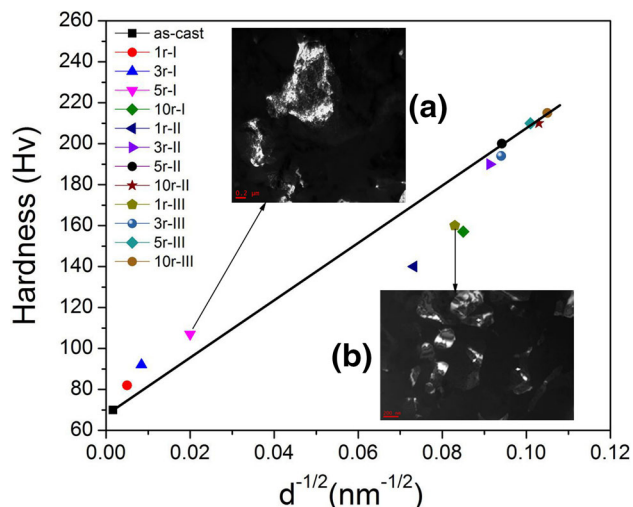
Fig. 5 The microstructure micrographs and the corresponding statistical distribution of the grain sizes from region III of the alloy after HPT treatment for (a, b) 1, (c, d) 3, (e, f) 5 and (g, h) 10 turns, respectively

grain boundaries led to a weaker strengthening effect for an austenitic stainless steel (Ref 30). For SPD processed materials, the grain boundaries differ in their misorientation angles as a

direct result of the microstructural evolution. Thus, as the applied strain increases, the distribution in the misorientation angles is shifted to higher values so that the fraction of HAGBs

Table 1 Average grain size of Al-4Mg alloy in three regions of the disks subjected to 0, 1, 3, 5, 10 turns

Turns	0		1		3		5		10	
	Average grain size	SD	Average grain size	SD	Average grain size	SD	Average grain size	SD	Average grain size	SD
Region I	400 μm	80 μm	40 μm	15 μm	14 μm	3 μm	2.5 μm	1 μm	138 nm	40 nm
Region II	185 nm	60 nm	120 nm	45 nm	110 nm	30 nm	95 nm	12 nm
Region III	145 nm	40 nm	110 nm	30 nm	100 nm	15 nm	90 nm	10 nm

**Fig. 6** The Hall-Petch relationship for coarse-grained samples and samples processed through various numbers of HPT turns. The insert TEM images are the microstructures for the samples after HPT treatment (a) at low strain and (b) medium strain

increases. According to a dislocation pile-up model (Ref 27), Armstrong (Ref 31) suggested the incipient plastic deformation as a process of dislocation source operation by the stress concentration at the grain boundary. Following the relationship between the stress concentration and the critical shear stress for source operation, the Hall-Petch coefficient K_H can be expressed as

$$K_H = 3m(\pi m_s \tau_c G b / 2\alpha)^{1/2}$$

where m is the Taylor factor relating the tensile strength to the resolved shear stress of a polycrystal, m_s is the Sachs orientation factor (Ref 32), G is the shear modulus, b is the Burgers vector, an average dislocation character is expressed in the factor $\alpha = 2(1 - \nu)/(2 - \nu)$, with ν being the Poisson's ratio, τ_c being the resolved shear stress required to operate the dislocation source near the grain boundary, and the ratio 3 being from the well-accepted Tabor's relation between indentation hardness and yield strength of a material (Ref 33). Thus, K_H is a function of the shear modulus, Burgers vector, Poisson's ratio and, in particular, the critical shear stress for dislocation nucleation from grain boundary. Previous study has shown that the resolved shear stress to move a full dislocation from a grain boundary into a grain is greater than the stress required to extend a partial dislocation into the same grain for f.c.c. metals (Ref 25, 34). Moreover, it is well known that critical stress (0.88 G) for partial dislocation nucleation is far higher than the stress for partial dislocation emission (Ref 35). The low angle grain boundaries include a lot of dislocations that do not need dislocation nucleation.

Therefore, they represent weaker barriers for the movement of lattice dislocations. With further increasing the strain, the non-equilibrium grain boundaries transform into equilibrium grain boundaries. And thus the hardness values fit the Hall-Petch relationship very well.

5. Conclusions

In this study, the structural evolution and structure-hardness relationship of an Al-4wt.%Mg alloy processed by HPT were investigated. Initially, the raw coarse grain is fragmented by the accumulation, interaction, tangling and spatial rearrangement of dislocations. Then, the obtained ultrafine grain is refined to several small domains under the high local stress with partial dislocation emission from the boundary between domains to accommodate further plastic strain. With partial dislocation emission from boundaries, the nanodomains gradually transform to nanograins. The presence of high density SFs in these nanodomains is due to the high flow stress from HPT processing. In addition, the Hall-Petch relation is not suitable for predicting the hardness of the targeted alloy. Firstly, dislocation between grain boundaries has an obvious influence on the hardness. Secondly, the low angle grain boundaries have a lower effect than that of the high angle grain boundaries to stop dislocation transfer through the grain boundaries.

Acknowledgments

The financial supports from National Natural Science Foundation of China (51531009), Grants from the Project of Innovation-driven Plan in Central South University (2015CX5003) and the outstanding graduate project of Advanced Non-ferrous Metal Structural Materials and Manufacturing Collaborative Innovation Center are appreciated. One of the authors (M. Song) would also thank the financial support from State Key Laboratory of Powder Metallurgy.

References:

1. M.A. Meyers, A. Mishra, and D.J. Benson, Mechanical Properties of Nanocrystalline Materials, *Prog. Mater. Sci.*, 2006, **51**(4), p 427–556
2. R.Z. Valiev and T.G. Langdon, Principles of Equal-Channel Angular Pressing as a Processing Tool for Grain Refinement, *Prog. Mater. Sci.*, 2006, **51**(7), p 881–981
3. A.P. Zhilyaev and T.G. Langdon, Using High-Pressure Torsion for Metal Processing: Fundamentals and Applications, *Prog. Mater. Sci.*, 2008, **53**(6), p 893–979
4. G. Liu, J. Gu, S. Ni, Y. Liu, and M. Song, Microstructural Evolution of Cu-Al Alloys Subjected to Multi-Axial Compression, *Mater. Charact.*, 2015, **103**, p 107–119

5. Y. Saito, N. Tsuji, H. Utsunomiya, T. Sakai, and R.G. Hong, Ultra-Fine Grained Bulk Aluminum Produced by Accumulative Roll-Bonding (ARB) Process, *Scr. Mater.*, 1998, **39**(9), p 1221–1227
6. M.I. Latypov, I.V. Alexandrov, Y.E. Beygelzimer, S. Lee, and H.S. Kim, Finite Element Analysis of Plastic Deformation in Twist Extrusion, *Comput. Mater. Sci.*, 2012, **60**, p 194–200
7. D. Orlov, Y. Beygelzimer, S. Synkov, V. Varyukhin, N. Tsuji, and Z. Horita, Plastic Flow, Structure and Mechanical Properties in Pure Al Deformed by Twist Extrusion, *Mater. Sci. Eng. A*, 2009, **519**(1–2), p 105–111
8. R.Z. Valiev, R.K. Islamgaliev, and I.V. Alexandrov, Bulk Nanostructured Materials from Severe Plastic Deformation, *Prog. Mater. Sci.*, 2000, **45**(2), p 103–189
9. Y. Estrin and A. Vinogradov, Extreme Grain Refinement by Severe Plastic Deformation: A Wealth of Challenging Science, *Acta Mater.*, 2013, **61**(3), p 782–817
10. M. Kawasaki, Different Models of Hardness Evolution in Ultrafine-Grained Materials Processed by High-Pressure Torsion, *J. Mater. Sci.*, 2014, **49**(1), p 18–34
11. I. Sabirov, M.Y. Murashkin, and R.Z. Valiev, Nanostructured Aluminium Alloys Produced by Severe Plastic Deformation: New Horizons in Development Mater, *Sci. Eng. A*, 2013, **560**(2), p 1–24
12. C. Huang, K. Wang, S. Wu, Z. Zhang, G. Li, and S. Li, Deformation Twinning in Polycrystalline Copper at Room Temperature and Low Strain Rate, *Acta Mater.*, 2006, **54**(3), p 655–665
13. X. Liao, Y. Zhao, Y. Zhu, R. Valiev, and D. Gunderov, Grain-Size Effect on the Deformation Mechanisms of Nanostructured Copper Processed by High-Pressure Torsion, *J. Appl. Phys.*, 2004, **96**(1), p 636–640
14. Z. Wang, Y. Wang, X. Liao, Y. Zhao, E. Lavernia, Y. Zhu, Z. Horita, and T. Langdon, Influence of Stacking Fault Energy on Deformation Mechanism and Dislocation Storage Capacity in Ultrafine-Grained Materials, *Scr. Mater.*, 2009, **60**(1), p 52–55
15. M. Chen, E. Ma, K.J. Hemker, H. Sheng, Y. Wang, and X. Cheng, Deformation Twinning in Nanocrystalline Aluminum, *Science*, 2003, **300**(5623), p 1275–1277
16. X. Liao, F. Zhou, E. Lavernia, S. Srinivasan, M. Baskes, D. He, and Y. Zhu, Deformation Mechanism in Nanocrystalline Al: Partial Dislocation Slip, *Appl. Phys. Lett.*, 2003, **83**(4), p 632–634
17. M. Liu, H. Roven, X. Liu, M. Murashkin, R. Valiev, T. Ungár, and L. Balogh, Grain Refinement in Nanostructured Al-Mg Alloys Subjected to HPT, *J. Mater. Sci.*, 2010, **45**(17), p 4659–4664
18. Z. Xu, N. Li, H. Jiang, and L. Liu, Deformation Nanotwins in Coarse-Grained Aluminum Alloy at Ambient Temperature and Low Strain Rate, *Mater. Sci. Eng. A*, 2015, **621**, p 272–276
19. Y. Cao, Y.B. Wang, X.Z. Liao, M. Kawasaki, S.P. Ringer, T.G. Langdon, and Y.T. Zhu, Applied Stress Controls the Production of Nano-Twins in Coarse-Grained Metals, *Appl. Phys. Lett.*, 2012, **101**(23), p 231903-1–231903-5
20. Y. Estrin, A. Molotnikov, C.H.J. Davies, and R. Lapovok, Strain Gradient Plasticity Modelling of High-Pressure Torsion, *J. Mech. Phys. Solids*, 2008, **56**(4), p 1186–1202
21. J.Y. Huang, Y.T. Zhu, H. Jiang, and T.C. Lowe, Microstructures and Dislocation Configurations in Nanostructured Cu Processed by Repetitive Corrugation and Straightening, *Acta Mater.*, 2001, **49**(9), p 1497–1505
22. X. Yang, S. Ni, and M. Song, Partial Dislocation Emission in a Superfine Grained Al-Mg Alloy Subject to Multi-axial Compression, *Mater. Sci. Eng. A*, 2015, **641**, p 189–193
23. V. Yamakov, D. Wolf, S.R. Phillpot, A.K. Mukherjee, and H. Gleiter, Dislocation Processes in the Deformation of Nanocrystalline Aluminum by Molecular-Dynamic Simulation, *Nat. Mater.*, 2002, **1**(1), p 45–49
24. R.J. Asaro, P. Krysl, and B. Kad, Deformation Mechanism Transitions in Nanoscale FCC Metals, *Philos. Mag. Lett.*, 2003, **83**(12), p 733–743
25. Y. Zhu, X. Liao, and X. Wu, Deformation Twinning in Nanocrystalline Materials, *Prog. Mater. Sci.*, 2012, **57**(1), p 1–62
26. J. Wang and H. Huang, Shockley Partial Dislocations to Twin: Another Formation Mechanism and Generic Driving Force, *Appl. Phys. Lett.*, 2004, **85**(24), p 5983–5985
27. E. Hall, The Deformation and Ageing of Mild Steel: III, Discussion of Results, *Proc. Phys. Soc. Lond. Sect. B*, 1951, **643**(9), p 747–752
28. N. Hansen, Hall-Petch Relation and Boundary Strengthening, *Scr. Mater.*, 2004, **51**(8), p 801–806
29. H.G.F. Wilsdorf and D. Kuhlmann-Wilsdorf, Work Softening and Hall-Petch Hardening in Extruded Mechanically Alloyed Alloys, *Mater. Sci. Eng. A*, 1993, **164**(1–2), p 1–14
30. K.J. Kurzydłowski, B. Ralph, J.J. Bucki, and A. Garbacz, The Grain Boundary Character Distribution Effect on the Flow Stress of Polycrystals: The Influence of Crystal Lattice Texture, *Mater. Sci. Eng. A*, 1996, **205**(1–2), p 127–132
31. R.W. Armstrong, Theory of the Tensile Ductile-Brittle Behavior of Poly-Crystalline HCP Materials, with Application to Beryllium, *Acta Metall.*, 1968, **16**(3), p 347–355
32. R. Armstrong, I. Codd, R. Douthwaite, and N. Petch, The Plastic Deformation of Polycrystalline Aggregates, *Philos. Mag.*, 1962, **7**(73), p 45–58
33. D. Wu, J. Zhang, J.C. Huang, H. Bei, and T.G. Nieh, Grain-Boundary Strengthening in Nanocrystalline Chromium and the Hall-Petch Coefficient of Body-Centered Cubic Metals, *Scr. Mater.*, 2013, **68**(2), p 118–121
34. L. Wang, H. Bei, T.L. Li, Y.F. Gao, E.P. George, and T.G. Nieh, Determining the Activation Energies and Slip Systems for Dislocation Nucleation in Body-Centered Cubic Mo and Face-Centered Cubic Ni Single Crystals, *Scr. Mater.*, 2011, **65**(3), p 179–182
35. Y.T. Zhu, X.Z. Liao, S.G. Srinivasan, Y.H. Zhao, M.I. Baskes, F. Zhou, and E.J. Lavernia, Nucleation and Growth of Deformation Twins in Nanocrystalline Aluminum, *Appl. Phys. Lett.*, 2004, **85**(21), p 5049–5051